Isoscalar and isovector density dependence of the pairing functional determined from global fitting

M. Yamagami,[1] J. Margueron,[2] H. Sagawa,[1] and K. Hagino[3]
[1]*Department of Computer Science and Engineering, University of Aizu, Aizu-Wakamatsu, Fukushima 965-8580, Japan*
[2]*Institut de Physique Nucléaire, Université Paris-Sud, IN2P3-CNRS, F-91406 Orsay Cedex, France*
[3]*Department of Physics, Tohoku University, Sendai, 980-8578, Japan*
(Received 13 March 2012; revised manuscript received 2 August 2012; published 24 September 2012)

We optimize the density dependence of a local energy density functional for pairing correlations (pair-DF), taking into account both the isoscalar and the isovector densities. All the experimental pairing gaps in even-even nuclei with $N, Z > 8$ are analyzed by performing the Hartree-Fock-Bogoliubov calculation. The new pairing energy density functionals give the best fit for all the pairing gaps with the rms deviation of $\sigma_{\rm tot} = (260–360)$ keV, depending on adopted Skyrme interactions in the particle-hole channel. It is shown that the isoscalar-density dependence in the pair-DF can be determined almost uniquely for the several Skyrme forces by adjusting the neutron and proton pairing gaps. An empirical relation among the parameters in the isoscalar part of pair-DF is extracted. The uncertainty of the isovector part is also examined by calculating the pairing gaps of neutron-rich and proton-rich nuclei in a wider region of the nuclear chart. We point out also that the linear isovector-density dependence in the pair-DF can mimic well the Coulomb effect for pairing correlations in neutron-rich nuclei. We discuss finally the predictive power of the pair-DF for pairing properties around drip-line regions.

DOI: 10.1103/PhysRevC.86.034333 PACS number(s): 21.60.Jz, 21.60.Ev, 21.10.Dr, 21.10.Re

I. INTRODUCTION

The low-energy nuclear properties are strongly influenced by the pairing correlation. In order to understand unstable nuclei that exist in celestial bodies and in a nuclear reactor, it is necessary to develop an effective interaction that allows one to reproduce the global pairing properties, that is, the dependence on the mass number A and on the neutron excess $\alpha = (N - Z)/A$.

In contrast to extensive efforts for improving the energy density functional (EDF) for the particle-hole channel [1], the pairing part (pair-DF) has not been well controlled. A promising procedure is a microscopic derivation of the pair-DF from a bare interaction by including both the medium polarization effect and the surface phonon coupling effect in finite nuclei. This progress continues steadily in spite of the massive computational effort [2–12].

A phenomenological construction with the aid of experimental data is also a promising strategy for constructing EDFs (see Refs. [13,14] for recent investigations). The parameters in the pair-DF are constrained by the requirement to reproduce the experimental data such as masses, low-lying excited states, and rotational properties. For this direction, the pair-DF, which depends only on the isoscalar density ($\rho = \rho_n + \rho_p$) [15–19], is widely employed.

It is to be noted that the functional form of the ρ dependence is still under discussion [20,21]. The ρ dependence has influence on the A dependence of the pairing gap [21,22], while the average trend of the experimental pairing gaps has dependence not only on A but also the neutron excess α [23]. In order to overcome this difficulty, in previous works we proposed a pair-DF including the linear [24–26] and quadratic isovector density ($\rho_1 = \rho_n - \rho_p$) terms and analyzed the medium-heavy mass region ($122 \leqslant A \leqslant 194$ and $0.08 < \alpha < 0.23$) [23].

In this work, we extend our previous study and analyze all the experimental pairing gaps in even-even nuclei with $N, Z > 8$ [27] for global fitting of parameters in the pair-DF with the ρ and ρ_1 terms. It is under debate whether a single pair-DF can describe pairing properties from the β-stable line to drip-line regions (for example, see Refs. [13,14,23]). We expect that the new pair-DF has better predicting power across the nuclear chart.

This paper is organized as follows. In Sec. II, the functional form of our pair-DF is discussed. The procedures for the parameter optimization are detailed. In Sec. III, we determine the parameters of our pair-DF by extensive Hartree-Fock-Bogoliubov (HFB) calculations with a Skyrme force. In Sec. IV, the uncertainties of the parameters are also estimated. In Sec. V, the Coulomb effect in the pairing channel are discussed.

II. MODEL

A. Parameterization of pair-DF

The α dependence of pairing gap in neutron-rich nuclei was pointed out by Vogel *et al.* [28] by analyzing the experimental data in the region of $50 < Z < 82$ and $82 < N < 126$. In Ref. [23], we extended the analysis with recently measured mass and found that the pairing gap can be empirically parameterized as

$$\bar{\Delta}_n^{(\rm exp)}(A, \alpha) = (1 - 7.74\,\alpha^2)\Delta_n^{(\rm A)}, \tag{1}$$

$$\bar{\Delta}_p^{(\rm exp)}(A, \alpha) = (1 - 8.25\,\alpha^2)\Delta_p^{(\rm A)}, \tag{2}$$

with the A-dependent parts $\Delta_n^{(\rm A)} = 6.75/A^{1/3}$ MeV and $\Delta_p^{(\rm A)} = 6.36/A^{1/3}$ MeV.

The microscopic origin of the α dependence is still under debate. The authors of Ref. [29] showed the reduction of the pairing gap toward the neutron drip line in Sn isotopes, based on a Thomas-Fermi calculation with the Gogny D1S force for both the particle-hole and pairing channels. In Ref. [28],

the authors considered the neutron-excess dependence of the particle-hole mean field (Lane potential) as a possible origin.

In order to distinguish the effects in the particle-hole channel and in the pairing channel, it is useful to carry out self-consistent HFB calculations with the isoscalar-density-dependent pairing force (for example, see Refs. [1,20])

$$H_{\rm pair}(\boldsymbol{r}) = \frac{V_0}{4}\left\{1-\eta_0\left[\frac{\rho(\boldsymbol{r})}{\rho_0}\right]^{\beta}\right\}\sum_{\tau=n,p}[\tilde{\rho}_\tau(\boldsymbol{r})]^2\,. \qquad (3)$$

Here, V_0 is the strength parameter, and $\rho_0 = 0.16$ fm^{-3} is the saturation density of the symmetric nuclear matter. The parameters η_0 and β control the isoscalar-density dependence of pairing force.

Apart from rending the weakened pairing correlations in the nuclear interior, the isoscalar-density dependence in Eq. (3) is not motivated by any arguments based on the microscopic theory of effective interaction. A pure two-body force ($\eta_0 = 0$) keeps some sensitivity of pairing to the nuclear interior while a density dependence with ($\eta_0 = 1$) pushes the sensitivity towards the outer surface.

The parameter η_0 has influence on the mass-number dependence of pairing gap. An intermediate value between the two extremes is adopted in Refs. [21,22]. The power of density, β, may affect the appearance of neutron skins and halos [22]. Since it is difficult to fix the value β using the available data, $\beta = 1$ is commonly adopted [1].

In Ref. [23], we performed self-consistent HFB calculation with Skyrme force in the particle-hole channel and pairing force of Eq. (3). We showed that the α dependence of the pairing gap cannot be reproduced unless the pair-DF incorporates the isovector-density dependence [23].

Utilization of the same Skyrme force for both in the particle-hole channel and in the particle-particle channel [30], or more general theories such as the density matrix expansion [31], provide the local energy density functional including various terms incorporating the isovector properties in the pairing channel.

The Skyrme SkP parametrization is a unique case for this direction, although the isovector properties do not seem well constrained for the α dependence of pairing gap (for example, see Fig. 22 in Ref. [20] for the calculation of neutron pairing gaps in Sn isotopes).

In order to reproduce the α dependence of pairing gap in the region of $50 < Z < 82$ and $82 < N < 126$ (which corresponds to zone 0 in Subsec. II B of the present study) by calculation with a local energy density functional, we proposed a pair-DF including not only a linear ρ dependence but also new terms depending on ρ_1 and ρ_1^2 in Ref. [23].

We intend to include the minimum set of the isoscalar- and isovector-density terms in the pair-DF for our propose. The complete investigation of various terms appearing in the density matrix expansion is not our present goal.

Therefore, we employ the functional form of

$$H_{\rm pair}(\boldsymbol{r}) = \frac{1}{4}\sum_{\tau=n,p} V_\tau\; g_\tau[\rho,\rho_1][\tilde{\rho}_\tau(\boldsymbol{r})]^2 \qquad (4)$$

with

$$g_\tau[\rho,\rho_1] = 1-\eta_0\frac{\rho(\boldsymbol{r})}{\rho_0}-\eta_1\frac{\tau_3\rho_1(\boldsymbol{r})}{\rho_0}-\eta_2\left[\frac{\rho_1(\boldsymbol{r})}{\rho_0}\right]^2. \qquad (5)$$

Here $\tau_3 = 1$ for $\tau = n$ (neutron) and -1 for p (proton). $\tilde{\rho}_\tau$ is the pair density. We call the pair-DF with only the ρ term (that is, $\eta_1 = \eta_2 = 0$) PDF-IS, that with the ρ and linear ρ_1 terms (that is, $\eta_2 = 0$) PDF-IV1, and that with all terms PDF-IV2.

Reference [25] introduced the linear ρ_1 term so as to simulate the neutron pairing gaps in symmetric and neutron matters. In Ref. [24], the linear ρ_1 term was considered to take into account the neutron skin effect on pairing. It was also pointed out that the parameter η_1 has a linear dependence on the isovector effective mass parameter of the particle-hole channel [23].

As we argue in Sec. V, the linear ρ_1 term can also simulate the Coulomb effect in the pairing channel. This allows us to make the strength parameters for the neutron and proton identical, that is, $V_0 = V_n = V_p$. This preserves the charge symmetry of the pair-DF.

The quadratic ρ_1 term is necessary so as to reproduce the α dependence of experimental pairing gaps [23].

In Ref. [23], these phenomenological terms were examined by analyzing experimental data in a limited region of the mass number and the neutron excess. In this paper, we re-examine the phenomenological terms by analyzing experimental data in a wider region.

B. Setup of analysis

The Skyrme SLy4 parametrization [32] is mainly used in the particle-hole channel of EDF in this work. To draw a general conclusion, we compare the results to those with other standard Skyrme parameters: SkM* [33], LNS [34], and SkP [30]. The computer code developed by Stoitsov *et al*. [35] is utilized. Starting from three different initial conditions, that is, the spherical, prolate, and oblate configurations, the lowest energy solution is searched for in the space of axially symmetric quadrupole deformation. The cutoff quasiparticle energy $E_{\rm cut} = 60$ MeV is fixed.

We analyze all the experimental pairing gaps of even-even nuclei with $Z, N > 8$ for optimization of the pair-DF. We divide the nuclear chart into four zones: zones 0, 1, 2, and 3. The definitions of zones are listed in Table I. Zone 0, adopted in Ref. [23], is now a part of zone 1, which includes nuclei being well apart from the closed shells. Zone 2 is the data set closer to the closed shells, and zone 3 includes only the data of semimagic nuclei as shown in Fig. 1. The histograms in Fig. 2 represent the distributions of the experimental data as a function of A and α in each zone.

In Ref. [23], the parameters (V_0, η_0, η_1, η_2) have been determined by analyzing a smaller set of data in the medium-heavy mass region called zone 0. In the present study, we determine the parameters in a wider region called zone 1. We check the performance of the pair-DF so obtained with near-semimagic nuclei (zone 2) and semimagic nuclei (zone 3).

The root-mean-square (rms) deviation of the result of the calculation from the experimental pairing gaps is evaluated in

TABLE I. Definition of zones 0, 1, 2, and 3 shown in Fig. 1. The $N^{(i)}_{\rm nucl}$ is the number of nuclei that have experimental data of neutron and/or proton pairing gaps, and the $N^{(i)}_n$ ($N^{(i)}_p$) represents the number of experimental neutron (proton) pairing gaps in zone i ($i = 0, 1, 2, 3$). The symbols $Z_{\rm mag}$ and $N_{\rm mag}$ are the nearest magic numbers, 20, 28, 50, 82, and 126.

	Region of N and Z	A	α	$N^{(i)}_{\rm nucl}$	$N^{(i)}_n$	$N^{(i)}_p$
Zone 0	Inside zone 1 restricted to $56 \leqslant Z \leqslant 76$	$122 \leqslant A \leqslant 194$	$0.08 < \alpha < 0.23$	94	93	84
Zone 1	$\lvert Z - Z_{\rm mag}\rvert \geqslant 6$ and $\lvert N - N_{\rm mag}\rvert \geqslant 6$	$24 \leqslant A \leqslant 254$	$-0.08 < \alpha < 0.24$	170	159	139
Zone 2	$2 \leqslant \lvert Z - Z_{\rm mag}\rvert \leqslant 4$ and $2 \leqslant \lvert N - N_{\rm mag}\rvert \leqslant 4$	$20 \leqslant A \leqslant 220$	$-0.09 < \alpha < 0.29$	216	211	191
Zone 3	Semimagic nuclei	$32 \leqslant A \leqslant 216$	$-0.05 < \alpha < 0.25$	69	40	29

each zone. The neutron, proton, and total rms deviations for zone i ($i = 0, 1, 2, 3$) are defined by

$$\sigma_\tau^{(\text{zone } i)} = \left[\frac{1}{N_\tau^{(i)}} \sum_{\text{Nuclei}\in\text{zone } i} \left(\Delta_\tau - \Delta_\tau^{(\text{exp})}\right)^2\right]^{1/2}, \quad (6)$$

$$\sigma_{\rm tot}^{(\text{zone } i)} = \left[\frac{1}{N_{\rm tot}^{(i)}} \sum_{\tau=n,p} \sum_{\text{Nuclei}\in\text{zone } i} \left(\Delta_\tau - \Delta_\tau^{(\text{exp})}\right)^2\right]^{1/2}, \quad (7)$$

where τ is n or p. The superscript of $\sigma^{(\text{zone } i)}$ indicates the zone where the fitting procedure is performed. The deviations $\sigma_{\rm tot}^{(\rm all)}$, $\sigma_n^{(\rm all)}$, and $\sigma_p^{(\rm all)}$ are obtained by analyzing all the data in zones 1 to 3.

The theoretical pairing gap is defined by Refs. [36–38]

$$\Delta_\tau = -\frac{\int d\boldsymbol{r}\tilde{\rho}_\tau(\boldsymbol{r})\tilde{h}_\tau(\boldsymbol{r})}{\int d\boldsymbol{r}\tilde{\rho}_\tau(\boldsymbol{r})}, \quad (8)$$

where the local pairing potential is given by

$$\tilde{h}_\tau(\boldsymbol{r}) = \frac{\delta}{\delta\tilde{\rho}_\tau(\boldsymbol{r})}\int d\boldsymbol{r}' H_{\rm pair}(\boldsymbol{r}'). \quad (9)$$

The $N_n^{(i)}$ ($N_p^{(i)}$) is the number of the experimental neutron (proton) pairing gaps in zone i, and $N_{\rm tot}^{(i)} = N_n^{(i)} + N_p^{(i)}$ is the sum. The experimental pairing gap $\Delta_\tau^{(\rm exp)}$ is extracted by the odd-even staggering of binding energy defined by the three-point formula $\Delta^{(3)}$. The theoretical pairing gap for even N is often compared with the experimental $\Delta^{(3)}$ for $N + 1$ [39]. In this work, we consider the average over the two gaps centered at neighboring odd isotopes: $\Delta_n^{(\rm exp)}(N) = [\Delta^{(3)}(N-1) + \Delta^{(3)}(N+1)]/2$ for each even N nucleus to eliminate the local fluctuations [13,21]. The same definition of $\Delta_p^{(\rm exp)}(Z)$ is used for each even Z nucleus.

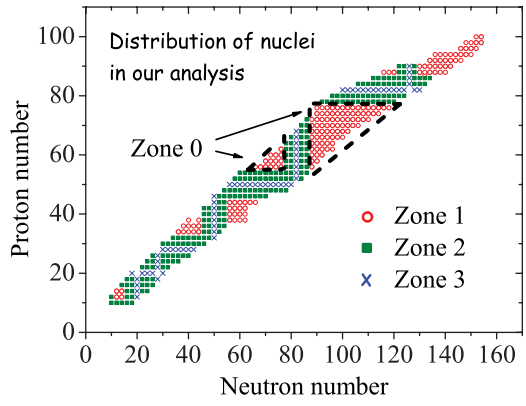

FIG. 1. (Color online) Experimental pairing gaps of even-even nuclei are grouped into zones 1, 2, and 3. The subset of zone 1, which we call zone 0, is also indicated. See text and Table I for the definitions.

C. Fitting procedure

We examine the four fitting procedures for determination of the four phenomenological parameters η_0, η_1, η_2, and $V_0 (= V_n = V_p)$. In order to demonstrate these procedures, an illustrative process at $\eta_0 = 0.75$ is shown in Table II. The Skyrme SLy4 is used in the particle-hole channel. The influence of the charge symmetry breaking $V_n \neq V_p$ is discussed in Sec. V.

1. The $V_0^{(^{156}\text{Dy})}$ procedure

This procedure was used in our previous analysis [23]. The $\sigma_{\rm tot}^{(\text{zone } 0)}$ is minimized by searching the optimal density dependence (η_0, η_1, η_2), while the strength V_0 is constrained

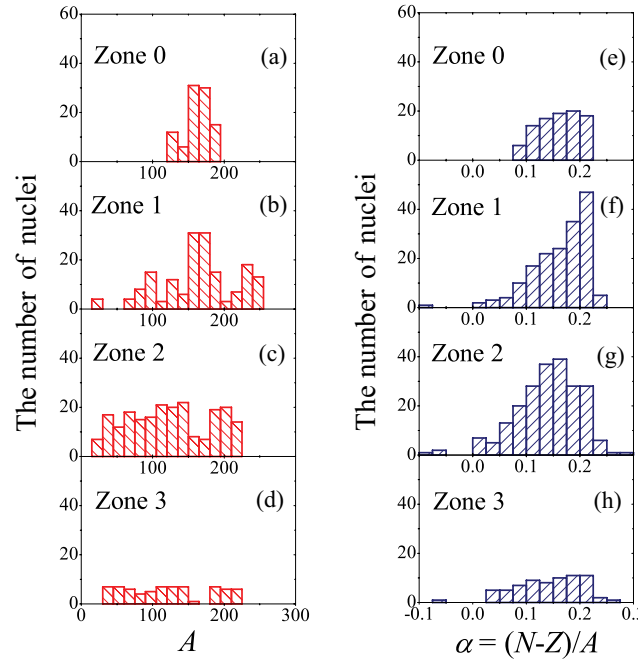

FIG. 2. (Color online) (Left) Distribution of experimental pairing gaps in each zone is shown as a function of A. (Right) The same data sets are plotted as a function of α.

TABLE II. The four fitting procedures for PDF-IV2 are demonstrated at fixed $\eta_0 = 0.75$. The strength parameter V_0 (MeV fm^{-3}) and the isovector-density dependences η_1 and η_2 are shown. The $\sigma_{\rm tot}^{(\rm zone\ 0)}$, $\sigma_{\rm tot}^{(\rm zone\ 1)}$, $\sigma_{\rm tot}^{(\rm zone\ 2)}$, $\sigma_{\rm tot}^{(\rm zone\ 3)}$, and $\sigma_{\rm tot}^{(\rm all)}$ (MeV) are also listed. The bold numbers indicate the result of each optimization procedure. The Skyrme SLy4 is used for the particle-hole channel. See the text for details.

SLy4 plus PDF-IV2 ($\eta_0 = 0.75$)										
Procedure	Condition for V_0	V_0	Condition for (η_1, η_2)	η_1	η_2	$\sigma_{\rm tot}^{(\rm zone\ 0)}$	$\sigma_{\rm tot}^{(\rm zone\ 1)}$	$\sigma_{\rm tot}^{(\rm zone\ 2)}$	$\sigma_{\rm tot}^{(\rm zone\ 3)}$	$\sigma_{\rm tot}^{(\rm all)}$
$V_0^{(^{156}\rm Dy)}$	$\Delta_n(^{156}\rm Dy)$	−434.07	Fit in zone 0	**0.270**	**2.5**	**0.186**	0.559	0.461	0.588	0.520
$V_0^{(\rm Zone\ 0)}$	Fit in zone 0	**−427.07**	Unchanged	0.270	2.5	**0.163**	0.493	0.386	0.508	0.450
Two-step	Fit in zone 1	**−396.47**	Unchanged	0.270	2.5	0.400	**0.333**	0.302	0.269	0.314
Direct	Fit in zone 1	**−396.26**	Fit in zone 1 with $\eta_2 = 2.5$	**0.390**	2.5	0.411	**0.324**	0.308	0.278	0.313

so as to reproduce the neutron pairing gap in ^{156}Dy. At fixed $\eta_0 = 0.75$, $(\eta_1, \eta_2) = (0.270, 2.5)$ is the optimal set.

2. The $V_0^{(\rm zone\ 0)}$ procedure

This procedure was also examined in Ref. [23]. The optimal V_0 is searched in zone 0, while the parameter set (η_0, η_1, η_2) is kept fixed to that determined by the $V_0^{(^{156}\rm Dy)}$ procedure. The improvement of $\sigma_{\rm tot}^{(\rm zone\ 0)}$ in this procedure compared to the $V_0^{(^{156}\rm Dy)}$ procedure is only 0.023 MeV. This means that the constraint to $\Delta_n(^{156}\rm Dy)$ is useful, if our analysis is restricted only to zone 0 [23].

However, the parameter set determined by the $V_0^{(\rm zone\ 0)}$ procedure gives large errors outside zone 0. For example, $\sigma_{\rm tot}^{(\rm zone\ 1)} = 0.493$ MeV is about three times larger than $\sigma_{\rm tot}^{(\rm zone\ 0)} = 0.163$ MeV with $V_0^{(\rm zone\ 0)}$ and $(\eta_0, \eta_1, \eta_2) = (0.75, 0.270, 2.5)$.

3. The two-step procedure

In this procedure, the strength V_0 is optimized in zone 1, while the parameter set (η_0, η_1, η_2) determined by the $V_0^{(^{156}\rm Dy)}$ procedure is unchanged. By changing from the $V_0^{(\rm zone\ 0)}$ procedure to the two-step procedure, although $\sigma_{\rm tot}^{(\rm zone\ 0)}$ gets 0.237 MeV worse, the improvements of $\sigma_{\rm tot}^{(\rm zone\ 1)}$, $\sigma_{\rm tot}^{(\rm zone\ 2)}$, and $\sigma_{\rm tot}^{(\rm zone\ 3)}$ are 0.160, 0.084, and 0.239 MeV respectively.

We notice that the $\sigma_{\rm tot}^{(\rm all)}$ decreases monotonically as 0.520, 0.450, and 0.314 MeV in calculations with the PDF-IV2, when changing the $V_0^{(^{156}\rm Dy)}$ procedure, the $V_0^{(\rm zone\ 0)}$ procedure, and the two-step procedure.

This desirable property may not be expected in other functional forms. For example, the $\sigma_{\rm tot}^{(\rm all)}$ with the pair-DF with the isoscalar-density dependence (PDF-IS) does not have this property, as is shown in Table III.

In our analysis, the common value $\eta_2 = 2.5$ is used for all sets of (V_0, η_0, η_1) and Skyrme forces. The applicability was checked in zone 0 for various Skyrme forces [23]. Here, we show that this is also the optimal value outside zone 0.

In order to justify this, the $\sigma_{\rm tot}^{(\rm all)}$ is plotted as a function of η_2 in Fig. 3. The SLy4 plus PDF-IV2 at $\eta_0 = 0.75$ is used. The parameters V_0 and η_1 are determined in a similar way as the two-step procedure: In the first step, η_1 is determined in zone 0 for given (η_0, η_2), while the V_0 is constrained by the neutron pairing gap of ^{156}Dy. Next, V_0 is optimized in zone 1 for given (η_0, η_1, η_2).

The $\sigma_{\rm tot}^{(\rm all)}$ is flat between $\eta_2 = 2.5$ and 4 and has the minimum around $\eta_2 = 3.5$, although this minimum is very shallow: The difference is $\sigma_{\rm tot}^{(\rm all)}(\eta_2 = 0) - \sigma_{\rm tot}^{(\rm all)}(\eta_2 = 2.5) = 0.035$ MeV, and the $\sigma_{\rm tot}^{(\rm all)}$ is insensitive for $\eta_2 \geqslant 2.5$.

D. Accuracy of two-step procedure

1. The direct procedure

The accuracy of the two-step procedure should be checked by extending the analysis in wider zones. Here, we consider the direct procedure in which the the strength V_0 and the density-dependence (η_0, η_1) are determined in zone 1 simultaneously. During the procedure, the parameter η_2 is fixed to be 2.5, because the $\sigma_{\rm tot}^{(\rm all)}$ has weak dependence on η_2 around 2.5 (see discussion in Subsec. II C).

The result of the direct procedure at $\eta_0 = 0.75$ is listed in Table II. The differences between the two-step procedure and the direct procedures are −0.011, 0.009, −0.006, and −0.009 MeV for $\sigma_{\rm tot}^{(\rm zone\ 0)}$, $\sigma_{\rm tot}^{(\rm zone\ 1)}$, $\sigma_{\rm tot}^{(\rm zone\ 2)}$, and $\sigma_{\rm tot}^{(\rm zone\ 3)}$

TABLE III. The three fitting procedures for PDF-IS are demonstrated at fixed $\eta_0 = 0.75$. The strength parameter V_0 (MeV fm^{-3}) of each procedure is shown. The $\sigma_{\rm tot}^{(\rm zone\ 0)}$, $\sigma_{\rm tot}^{(\rm zone\ 1)}$, $\sigma_{\rm tot}^{(\rm zone\ 2)}$, $\sigma_{\rm tot}^{(\rm zone\ 3)}$, and $\sigma_{\rm tot}^{(\rm all)}$ (MeV) are also listed. The bold numbers indicate the result of each optimization procedure. The Skyrme SLy4 is used for the particle-hole channel. See the text for details.

SLy4 plus PDF-IS ($\eta_0 = 0.75$)							
Procedure	Condition for V_0	V_0	$\sigma_{\rm tot}^{(\rm zone\ 0)}$	$\sigma_{\rm tot}^{(\rm zone\ 1)}$	$\sigma_{\rm tot}^{(\rm zone\ 2)}$	$\sigma_{\rm tot}^{(\rm zone\ 3)}$	$\sigma_{\rm tot}^{(\rm all)}$
$V_0^{(^{156}\rm Dy)}$	$\Delta_n(^{156}\rm Dy)$	−401.21	0.305	0.530	0.354	0.406	0.449
$V_0^{(\rm zone\ 0)}$	Fit in zone 0	**−407.27**	**0.289**	0.575	0.383	0.458	0.487
$V_0^{(\rm zone\ 1)}$	Fit in zone 1	**−370.80**	0.502	**0.432**	0.417	0.251	0.412

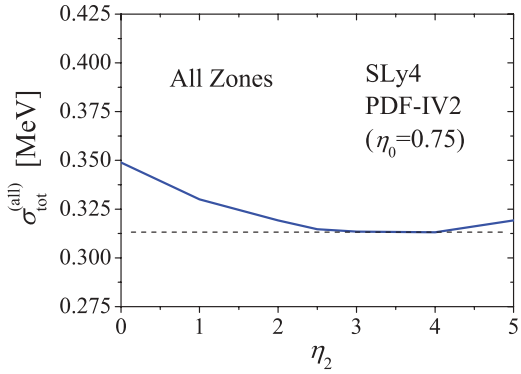

FIG. 3. (Color online) The $\sigma_{\rm tot}^{\rm (all)}$ is shown as a function of η_2. Here $\eta_0 = 0.75$ is fixed. The parameters η_1 and V_0 for SLy4 plus PDF-IV2 are optimized for each η_2. See text for details.

respectively. As a result, the $\sigma_{\rm tot}^{\rm (all)}$ of these procedures coincide within 0.001 MeV.

In order to understand the reason for the good agreement, we consider the $\sigma_{\rm tot}^{\rm (zone\ 1)}$ as functions of V_0 and η_1, while $\eta_0 = 0.75$ and $\eta_2 = 2.5$ are fixed. The V_0 dependence of $\sigma_{\rm tot}^{\rm (zone\ 1)}$ is shown in Fig. 4(a), where the results with $\eta_1 = 0.27$ (the optimal value in the two-step procedure) and $\eta_1 = 0.39$ (the optimal value in the direct procedure) are compared. This analysis shows that the strength parameter can be determined accurately due to the strong V_0 dependence.

On the other hand, the η_1 parameter has large uncertainty when changing the analyzed zones. This is shown in Fig. 4(b). Here, V_0 is optimized in zone 1 for given (η_0, η_1, η_2). The curve of $\sigma_{\rm tot}^{\rm (zone\ 1)}$ is shallow as a function of η_1.

The difference of η_1 in the two-step procedure and the direct procedure can be related to the distribution of nuclei used for the fit. In zone 1, used in the direct procedure, the distribution of pairing gaps versus α peaks at large values of α as shown in Fig. 2, while it is more flat in the case of zone 0, used in the two-step procedure. The direct procedure gives therefore more weight to nuclei with larger neutron excess and pushed η_1 to higher values than those obtained from the two-step procedure.

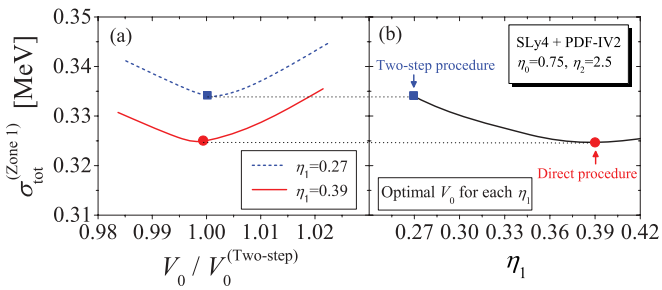

FIG. 4. (Color online) (Left) $\sigma_{\rm tot}^{\rm (zone\ 1)}$ is shown as a function of V_0. The results with $\eta_1 = 0.270$ and 0.390 are compared. Here $\eta_0 = 0.75$ and $\eta_2 = 2.5$ are fixed, and $V_0^{\rm (two\text{-}step)} = -396.47$ MeV fm^{-3}. The filled box and circle represent the minimum values of $\sigma_{\rm tot}^{\rm (zone\ 1)}$ in the two-step and direct procedures respectively. The Skyrme SLy4 and PDF-IV2 are used. (Right) The $\sigma_{\rm tot}^{\rm (zone\ 1)}$ is shown as a function of η_1. The V_0 is optimized in zone 1 for each η_1.

The good agreement of the rms deviations between the two fitting procedures guarantees the accuracy of the two-step procedure in our analysis. However, this implies that our pair-DF has freedom in η_1 value to improve the description power with future experimental data of more neutron-rich nuclei and possible extensions of the functional form.

Finally, we estimate the numerical task of our fitting procedures in order to show a computational advantage of the two-step procedure. To perform the HFB calculation for 170 nuclei in zone 1 (we call one iteration), it takes about 26 hours on a single CPU of the Altix3700 BX2 computer at the Yukawa Institute for Theoretical Physics in Kyoto University. This is estimated as follows: 170 [nuclei] × 3 [spherical, prolate, oblate initial conditions] × about 3 minutes [convergence from one initial condition] = about 26 hours.

In the two-step procedure, the strong V_0 dependence of the rms deviation requires typically 10 iterations for the five-digit accuracy of V_0. In the direct procedure, a few dozen iterations for each V_0 are additionally needed for the three-digit accuracy of η_1: A few hundred days are required on a single CPU for each η_0, in spite of the negligible improvement of the rms deviations. Therefore, the direct procedure consumes much more computer time and can be applied only for a limited region of the value η_0.

III. OPTIMIZATION OF PAIR-DF

A. Unique determination of ρ dependence

$\sigma_{\rm tot}^{\rm (all)}$, $\sigma_n^{\rm (all)}$, and $\sigma_p^{\rm (all)}$ are shown as functions of η_0 in Fig. 5. The parameters of PDF-IV2 are determined by the two-step procedure. The Skyrme SLy4 parametrization is used for the particle-hole channel. For comparison, we also plot the result of the direct procedure by open circles. Here, the parameters η_1 and V_0 are determined simultaneously for each η_0 in zone 1. Details of the direct procedure are given in Sec. II C and Table II.

We investigate the η_0 dependence of $\sigma_{\rm tot}^{\rm (all)}$ for improving the reproduction power of the A dependence of pairing gaps. As

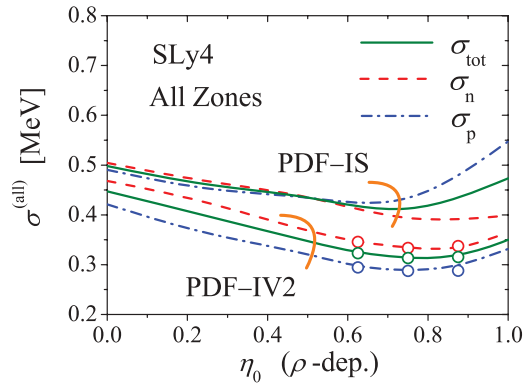

FIG. 5. (Color online) $\sigma_{\rm tot}^{\rm (all)}$, $\sigma_n^{\rm (all)}$, and $\sigma_p^{\rm (all)}$ are shown as functions of η_0. The SLy4 and the PDF-IV2 determined by the two-step procedure are used to draw the curves. The direct procedure is also performed at $\eta_0 = 0.625$, 0.750, and 0.875 and the results are marked by the open circles. The results with PDF-IS are also shown.

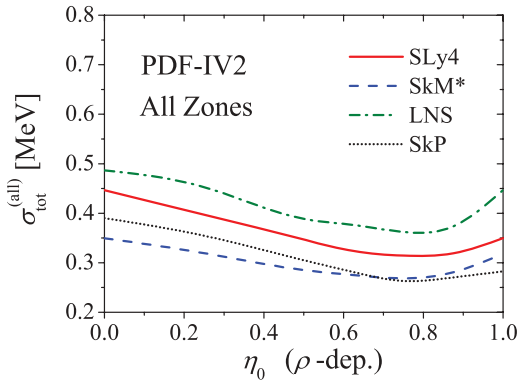

FIG. 6. (Color online) Comparison of $\sigma_{tot}^{(all)}$ with SLy4, SkM*, LNS, and SkP. The PDF-IV2 determined by the two-step procedure is used.

shown in Fig. 5, $\sigma_{tot}^{(all)}$ with PDF-IV2 gradually decreases as a function of η_0 and reaches the minimum at $\eta_0 = 0.75$. $\sigma_n^{(all)}$ and $\sigma_p^{(all)}$ also have the minimums at the same point $\eta_0 = 0.75$ simultaneously. This tendency can be obtained by the linear ρ_1 term in the pair-DF, while the contribution of the quadratic ρ_1 term is small (see Fig. 3).

To clarify the role of the ρ_1 dependence, $\sigma_{tot}^{(all)}$, $\sigma_n^{(all)}$, and $\sigma_p^{(all)}$ obtained with PDF-IS without ρ_1 terms are also plotted in Fig. 5. Here the V_0 is optimized for each η_0 in zone 1. $\sigma_n^{(all)}$ and $\sigma_p^{(all)}$ decrease as a function of η_0 up to around $\eta_0 = 0.7$. For larger η_0, on the other hand, only $\sigma_n^{(all)}$ has a plateau, while $\sigma_p^{(all)}$ increases due to the artificial quenching of Δ_p attributed to the neutron skin effect [24]: The growth of the neutron skin reduces the overlap between the form factor $[1 - \eta_0\rho(\boldsymbol{r})/\rho_0]$ and $\tilde{\rho}_p(\boldsymbol{r})$. Therefore $\sigma_n^{(all)}$ and $\sigma_p^{(all)}$ give different constraints on the parameter η_0 in the case of PDF-IS. This shortcoming of PDF-IS is solved by introducing the ρ_1 dependence as shown in Fig. 5 as $\sigma_n^{(all)}$ and $\sigma_p^{(all)}$ are simultaneously changed as a function of η_0 with the PDF-IV2.

We also perform the same analysis with other Skyrme parametrizations: SkM*, LNS, and SkP. The results are compared in Fig. 6. It is clearly seen that the minima of $\sigma_{tot}^{(all)}$ are at about $\eta_0 = 0.75$ in these Skyrme forces, although the absolute value of $\sigma_{tot}^{(all)}$ at the minimum depends on the particle-hole interaction. This result supports the unique determination of the ρ dependence and the pairing properties around the nuclear surface. The parameters of the pair-DF and the rms deviations at $\eta_0 = 0.75$ are given in Table IV.

TABLE IV. The parameter sets of PDF-IV2 at $(\eta_0, \eta_2) = (0.75, 2.5)$ for SLy4, SkM*, LNS, and SkP. The two-step procedure is performed. $\sigma_{tot}^{(all)}$, $\sigma_n^{(all)}$, $\sigma_p^{(all)}$ are listed. m_s^*/m is the isoscalar effective mass parameter of the Skyrme force.

Skyrme	(m_s^*/m)	V_0	η_1	$\sigma_{tot}^{(all)}$	$\sigma_n^{(all)}$	$\sigma_p^{(all)}$
SLy4	(0.69)	−396.47	0.270	0.314	0.334	0.289
SkM*	(0.79)	−371.60	0.427	0.268	0.282	0.251
LNS	(0.83)	−388.60	0.400	0.362	0.365	0.359
SkP	(1.00)	−317.50	0.300	0.264	0.297	0.218

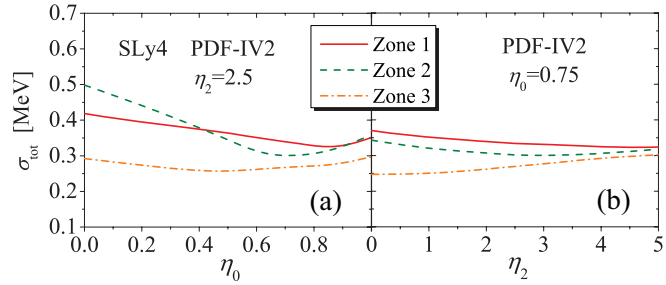

FIG. 7. (Color online) (a) $\sigma_{tot}^{(zone\ 1)}$, $\sigma_{tot}^{(zone\ 2)}$, and $\sigma_{tot}^{(zone\ 3)}$ are shown as a function of η_0. Here $\eta_2 = 2.5$ is fixed. The parameters η_1 and V_0 for SLy4 plus PDF-IV2 are determined by the two-step procedure. (b) The same figure with Fig. 7(a) but plotted as a function of η_2. Here $\eta_0 = 0.75$ is fixed.

B. Zone dependence

To check the performance of the pair-DF, we show σ_{tot} in zones 1, 2, and 3 separately in Fig. 7(a). Here SLy4 and PDF-IV2 are used. It is clear that the better minimum is obtained in zone 2, zone 1 has a less pronounced minimum, and the pairing gaps in zone 3 for semimagic nuclei give almost no constraint on η_0.

To understand the reason, the difference of the pairing gaps, $\delta\Delta_\tau = \Delta_\tau(\eta_0 = 0.75) - \Delta_\tau(\eta_0 = 0)$, is evaluated for each nuclei in zone 3. The result obtained with SLy4 and PDF-IV2 is shown as a function of A in Fig. 8. We notice that the dominant proportion of nuclei in zone 3 have $A > 100$, and the A dependence of pairing gap is weak in this A region due to the trend of $\Delta_\tau^{(exp)} \propto A^{-1/3}$. This fact causes the weak η_0 dependence of $\sigma_{tot}^{(zone\ 3)}$.

The correlations beyond the mean-field calculation may also contribute to the peculiar behavior in zone 3. The authors of Ref. [40] considered that the different behavior in semimagic nuclei may be partly attributed to the effect of the particle number fluctuation. They showed that the HFB calculation with the approximate particle number projection using the Lipkin-Nogami method improves the agreement with experiment for spherical nuclei. We leave it as an open problem to construct the pair-DF, which allows one to describe the

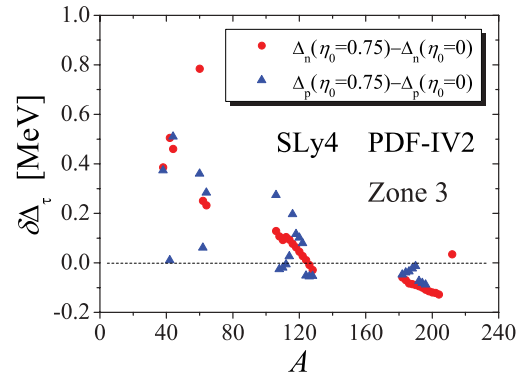

FIG. 8. (Color online) The difference of pairing gaps obtained with $\eta_0 = 0$ and $\eta_0 = 0.75$ for each nucleus. The result in zone 3 is plotted as a function of A. The SLy4 and PDF-IV2 determined by the two-step procedure are used.

pairing properties along the chains of semimagic nuclei in the same quality achieved for the deformed region [13,23,40–42].

We also plot $\sigma_{\rm tot}^{(\rm zone\ 1)}$, $\sigma_{\rm tot}^{(\rm zone\ 2)}$, and $\sigma_{\rm tot}^{(\rm zone\ 3)}$ separately as a function of η_2 in Fig. 7(b). The SLy4 and the PDF-IV2 at $\eta_0 = 0.75$ are used. It is seen that $\sigma_{\rm tot}^{(\rm zone\ 1)}$ and $\sigma_{\rm tot}^{(\rm zone\ 2)}$ have the same tendency as $\sigma_{\rm tot}^{(\rm all)}$. On the other hand, $\sigma_{\rm tot}^{(\rm zone\ 3)}$ increases as a function of η_2. This peculiar behavior in zone 3 is caused by the lack of experimental data in order to extract the neutron-excess dependence. To see this, the neutron pairing gaps in Ca, Ni, Sn, and Pb isotopes obtained with PDF-IS, PDF-IV1, and PDF-IV2 at $\eta_0 = 0.75$ are compared in Fig. 9.

The reduction effect for neutron pairing correlations due to the quadratic ρ_1 term is stronger than that due to the linear ρ_1 term in nuclei with large neutron excess. This is seen by comparing the results with PDF-IV1 and PDF-IV2. However, this effect is not visible in the experimental data due to the vanishing pairing gaps around the magic numbers; $N = 28, 50, 82$, and 126 in Ca, Ni, Sn, and Pb respectively. The tendency of reducing neutron pairing gaps toward the neutron drip line is also discussed in Ref. [29] by performing the Thomas-Fermi calculation with the Gogny force.

The same analysis but for the proton pairing gaps in $N = 20, 28, 50$, and 82 isotones is also shown in Fig. 9. In the proton case, the linear ρ_1 term enhances the proton pairing gaps, while the quadratic ρ_1 term reduces them. The sizable quenching effect due to the quadratic term can be seen also in nuclei with large neutron excess: $Z < 12$ in $N = 20$ isotones, $Z < 14$ in $N = 28$ isotones, $Z < 28$ in $N = 50$ isotones, and $Z < 50$ in $N = 82$ isotones.

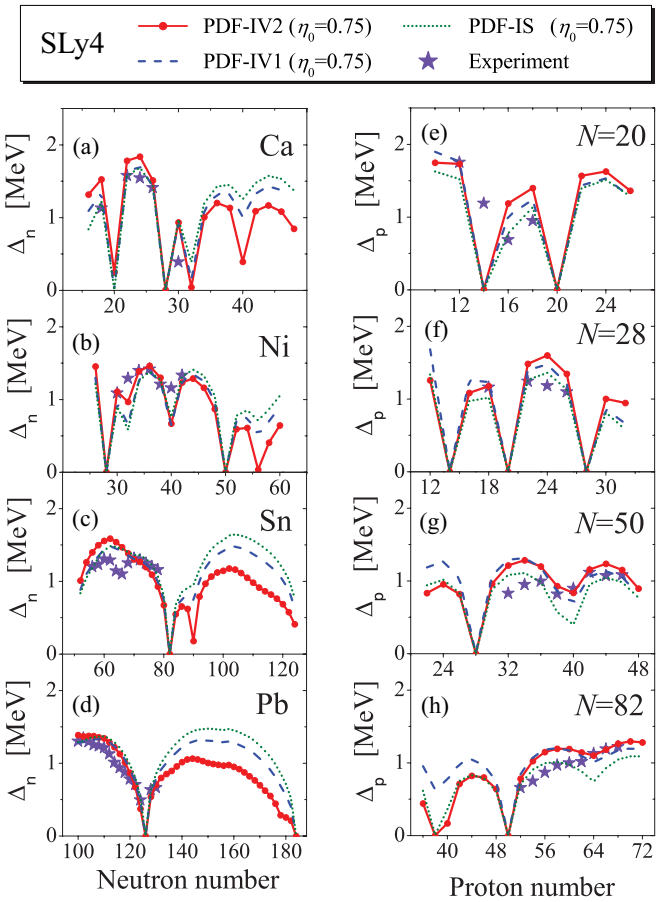

FIG. 9. (Color online) The neutron pairing gaps in Ca, Ni, Sn, and Pb isotopes (left) and the proton pairing gaps in $N = 20$, 28, 50, and 82 isotones (right). The results obtained with PDF-IS, PDF-IV1, and PDF-IV2 at $\eta_0 = 0.75$ are compared. The two-step procedure is performed. The experimental pairing gaps are also shown.

IV. UNCERTAINTIES IN PAIR-DF

A. Empirical expression for V_0

Pairing correlations are sensitive to the single-particle structure around the Fermi level [43]. The connections between effective interactions in the particle-hole and particle-particle channels can be expected. In the previous study [23], we showed the two relations: (1) the linear relation between the pairing strength V_0 and the isoscalar effective mass m_s^*/m of the Skyrme force and (2) the linear relation between the isovector-density dependence η_1 and the isovector effective mass m_v^*/m of the Skyrme force. Here, m_s^*/m and m_v^*/m [1]

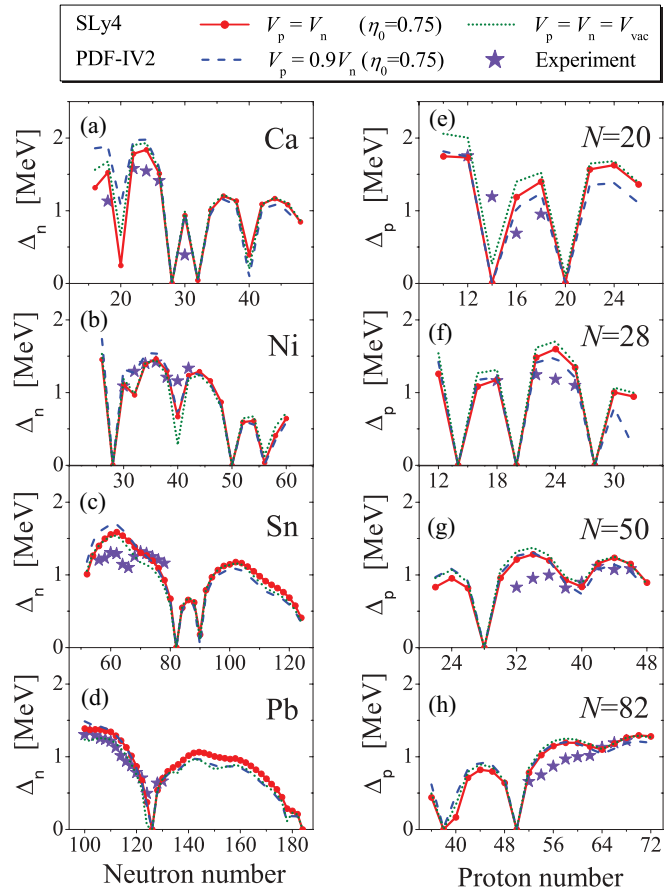

FIG. 10. (Color online) The same as in Fig. 9, but the results obtained by the PDF-IV2 with the optimized strengths under the assumption $V_p = V_n$ and $V_p = 0.9V_n$, and the fixed $V_p = V_n = V_{\rm vac}$ are compared. See the text for details.

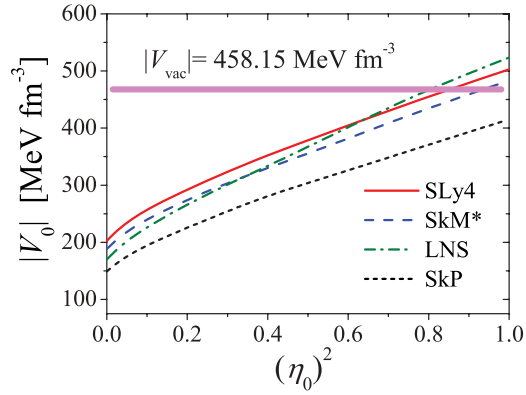

FIG. 11. (Color online) The parameters V_0 of PDF-IV2 for SLy4, SkM*, LNS, and SkP are shown as functions of $(\eta_0)^2$. The two-step procedure is performed.

are defined by

$$\frac{m}{m_s^*(\mathbf{r})} = 1 + \frac{2m}{\hbar^2}\left(b_1 - \frac{b_1'}{2}\right)\rho \tag{10}$$

$$\frac{m}{m_v^*(\mathbf{r})} = 1 + \frac{2m}{\hbar^2} b_1 \rho. \tag{11}$$

The b_1 and b_1 are combinations of Skyrme-force parameters t_1, t_2, x_1, and x_2:

$$b_1 = \tfrac{1}{8}[t_1(2+x_1) + t_2(2+x_2)] \tag{12}$$

$$b_1' = \tfrac{1}{8}[t_1(1+2x_1) - t_2(1+2x_2)]. \tag{13}$$

In this section, we extract empirical correlations among V_0, η_0, and m_s^*/m for PDF-IV2. For this purpose, the V_0 for SLy4, SkM*, LNS, and SkP are plotted as a function of $(\eta_0)^2$ in Fig. 11. The two-step procedure is performed. The V_0 has linear dependence on $(\eta_0)^2$ except for $(\eta_0)^2 < 0.1$. The slope can be parameterized commonly as $|V_0| = 260.58(\eta_0)^2 + f(m_s^*/m)$ MeV fm^{-3} for SLy4, SkM*, and SkP. In the LNS case, the slope is steeper: $|V_0| = 327.75(\eta_0)^2 + f(m_s^*/m)$ MeV fm^{-3}. Here $f(m_s^*/m)$ is a function of m_s^*/m.

$f(m_s^*/m)$ has linear dependence on m_s^*/m, and the coefficients were determined in zone 0 by analyzing 13 Skyrme forces in Ref. [23]. In the present study, we analyze the strength parameters determined by the two-step procedure. By fitting to the results shown in Fig. 12, we obtain the η_0 and m_s^*/m dependence:

$$|V_0| = 260.58(\eta_0)^2 - 255.18\frac{m_s^*}{m} + 418.59 \text{ MeV fm}^{-3}. \tag{14}$$

B. Constraint by low-density limit

It is desirable that a single EDF can describe nuclear properties from β-stability line to drip-line regions. For the description of drip-line nuclei, the density-dependent contact force is often used for the nuclear part of pairing interaction and the strength parameter is determined so as to reproduce the neutron-neutron (nn) scattering length a_{nn},

$$V_{\text{vac}} = \frac{2\pi^2\hbar^2}{m}\frac{2a_{nn}}{\pi - 2a_{nn}k_{\text{cut}}}. \tag{15}$$

TABLE V. The parameters set of PDF-IV2 for SLy4, SkM*, LNS, and SkP determined under the assumption $V_0 = V_{\text{vac}}$ and $\eta_2 = 2.5$. The optimization procedure for (η_0, η_1) is performed in zone 1. The $\sigma_{\text{tot}}^{(\text{all})}$, $\sigma_n^{(\text{all})}$, and $\sigma_p^{(\text{all})}$ are also compared.

Skyrme	(m_s^*/m)	η_0	η_1	$\sigma_{\text{tot}}^{(\text{all})}$	$\sigma_n^{(\text{all})}$	$\sigma_p^{(\text{all})}$
SLy4	(0.69)	0.903	0.483	0.322	0.345	0.293
SkM*	(0.79)	0.942	0.600	0.300	0.314	0.282
LNS	(0.83)	0.875	0.612	0.374	0.401	0.340
SkP	(1.00)	1.095	0.700	0.309	0.344	0.261

Here $k_{\text{cut}} = \sqrt{mE_{\text{cut}}/\hbar^2}$ with a cutoff energy E_{cut}. The $a_{nn} = -18.5$ fm [44] and the $E_{\text{cut}} = 60$ MeV give the strength $V_{\text{vac}} = -458.15$ MeV fm^{-3}. This procedure has been used in the three-body model [17,45–48] and the nuclear matter calculation [25,49].

We can infer the optimal value of η_0 for a given V_0 using Eq. (14). By substituting $V_0 = V_{\text{vac}} = -458.15$ MeV fm^{-3} into the empirical expression, we obtain $\eta_0^{(\text{empirical})} = 0.909$, 0.962, 0.900, and 0.988 for SLy4, SkM*, LNS, and SkP respectively.

It is worth mentioning that $\sigma_{\text{tot}}^{(\text{all})}$ is shallow from the minimum point to $\eta_0^{(\text{empirical})}$ along the η_0 direction for each Skyrme force (see Fig. 6). This may suggest a need for additional constraint for our pair-DF.

We examine the validity of the assumption $V_0 = V_{\text{vac}}$ by analyzing $\sigma_{\text{tot}}^{(\text{all})}$. The parameter set (η_0, η_1) of PDF-IV2 is optimized in zone 1 under the assumption $V_0 = V_{\text{vac}}$. During the procedure, $\eta_2 = 2.5$ is fixed.

The minimum values of $\sigma_{\text{tot}}^{(\text{all})}$ and the parameter set for each Skyrme force are listed in Table V. The difference of $\sigma_{\text{tot}}^{(\text{all})}$ with the results of the two-step procedure is less than 0.05 MeV (0.008, 0.032, 0.012, and 0.045 MeV for SLy4, SkM*, LNS, and SkP, respectively). In addition, the optimal

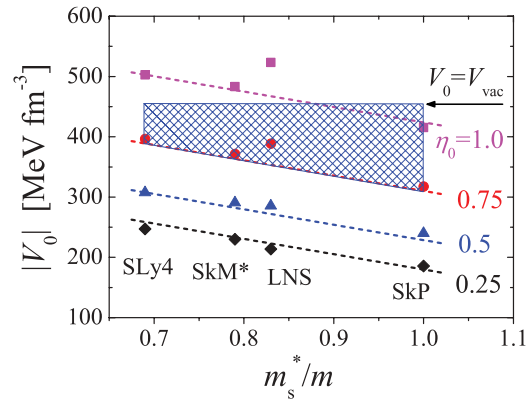

FIG. 12. (Color online) The optimal values of V_0 at $\eta_0 = 0.25$, 0.5, 0.75, and 1.0 are shown as functions of m_s^*/m. The two-step procedure is performed. The dashed lines represent the extracted relation $|V_0| = 260.58(\eta_0)^2 - 255.18m_s^*/m + 418.59$ MeV fm^{-3}. The shaded region indicates the uncertainty of parameters in the isoscalar part of PDF-IV2. $\sigma_{\text{tot}}^{(\text{all})}$ differs less than 0.05 MeV from the minimum value for each Skyrme force if (V_0, η_0) is in the shaded region. See the text for details.

values of the isoscalar-density dependence are also close to the empirical values $\eta_0^{(\mathrm{empirical})}$ as expected.

The empirical expression Eq. (14) and the comparison between the fitting procedures with or without the constraint $V_0 = V_{\mathrm{vac}}$ give a possible estimation of uncertainties in the phenomenological parameters in our pair-DF. The uncertainty of V_0 in connection with m_s^*/m and η_0 is indicated by the shaded region in Fig. 12.

The lower boundary of $|V_0|$ is determined by $\eta_0 = 0.75$ in the two-step procedure (see Fig. 6). The upper boundary is $|V_0| = |V_{\mathrm{vac}}|$, and the corresponding value of η_0 can be estimated by Eq. (14). For each Skyrme force, the parameter set in this shaded region gives less than 0.05 MeV difference in $\sigma_{\mathrm{tot}}^{(\mathrm{all})}$ (see Tables IV and V).

The upper boundary for $|V_0|$ is equivalent to a condition that our pair-DF should be attractive inside nuclei. Here, we show this for nuclei with $\alpha > 0$ (the same discussion can be applied for nuclei with $\alpha < 0$).

The attractive condition for our pair-DF of Eq. (4) can be written by

$$g_p > g_n \geqslant 1 - \eta_0 - \eta_1 \alpha_{\max} - \eta_2 \alpha_{\max}^2 \geqslant 0. \tag{16}$$

Here, $\rho \leqslant \rho_0$ and $\rho_1 \leqslant \alpha\rho_0$ are used. The maximum neutron excess is $\alpha_{\max} \approx 0.3$ in this study. This condition gives an inequality for η_0,

$$\eta_0 \leqslant 1 - \eta_1 \alpha_{\max} - \eta_2 \alpha_{\max}^2 < 1 - \eta_1 \alpha_{\max}. \tag{17}$$

By inserting this inequality into Eq. (14), we obtain

$$\begin{aligned} |V_0| &< 260.58(1 - \eta_1 \alpha_{\max})^2 - 255.18 \frac{m_s^*}{m} + 418.59 \\ &\leqslant 462.59\ (\mathrm{SLy4}) \approx |V_{\mathrm{vac}}|. \end{aligned} \tag{18}$$

For the estimation of the last line, we use the results of the two-step procedure: $\eta_1 \geqslant 0.27$ (SLy4), 0.427 (SkM*), 0.400 (LNS), and 0.300 (SkP) for $\eta_0 \geqslant 0.75$ (see Table IV).

We advocate the use of the pair-DF determined by the two-step procedure. This is because the value of $\sigma_{\mathrm{tot}}^{(\mathrm{all})}$ is minimal in this procedure. However, the synthetic use of experimental observables having sensitivity to pairing properties in the nuclear surface region may be promising for more accurate determination of the parameters: for example, neutron halos [22,50], dineutron correlations [17,51], pairing vibrations and two-neutron transfer reactions [52–56], and the isoscalar giant monopole resonances [57]. The further extension of the functional form may be also required for the accurate determination of the parameters (see discussion in Subsec. II A). These investigations remain for future studies.

V. COULOMB EFFECT

The repulsive Coulomb force weakens the pairing correlations. The 20–30% reduction of the proton pairing gap by the self-consistent treatment of the Coulomb force was reported in Refs. [58,59]. In Ref. [60], the authors proposed a prescription in which the explicit Coulomb effect can be taken into account by reducing V_p by about 10% for a wide range of mass number and neutron excess. This is shown by performing a fully self-consistent HFB calculation with Gogny force and the Coulomb force. A similar prescription has been found to work also for a three-body model calculation for the ^{17}Ne nucleus [48].

TABLE VI. The parameter sets of PDF-IV2 optimized under the assumption $V_p = 0.9V_n$ and $V_p = V_n$ are compared. Here $(\eta_0, \eta_2) = (0.75, 2.5)$ is fixed, and the two-step procedure is performed. $\sigma_{\mathrm{tot}}^{(\mathrm{all})}$, $\sigma_n^{(\mathrm{all})}$, and $\sigma_p^{(\mathrm{all})}$ are also listed.

Skyrme	V_p/V_n	V_n	η_1	$\sigma_{\mathrm{tot}}^{(\mathrm{all})}$	$\sigma_n^{(\mathrm{all})}$	$\sigma_p^{(\mathrm{all})}$
SLy4	0.90	−415.28	0.585	0.322	0.325	0.317
SLy4	1.00	−396.47	0.270	0.314	0.334	0.289

In most Skyrme EDF calculations so far, the pair-DF with only ρ dependence has been adopted. Instead of the explicit treatment of the Coulomb force, the parameters V_n and V_p are adjusted. The strength V_p is substantially stronger than V_n to reproduce the observed pairing properties [13,14,40,61].

On the other hand, we obtain smaller $\sigma_p^{(\mathrm{all})}$ than $\sigma_n^{(\mathrm{all})}$ by assuming $V_p = V_n$ for PDF-IV2 (see Table IV). In order to resolve the contradiction in the Skyrme EDF calculations, we investigate the role of the linear ρ_1 term in PDF-IV2 by comparing two assumptions: One is $V_p = V_n$. The other is $V_p = 0.9V_n$ in order to take into account the Coulomb effect within the local density approximation (the preliminary result is shown in Ref. [62]).

For the global comparison, we compare $\sigma_{\mathrm{tot}}^{(\mathrm{all})}$, $\sigma_n^{(\mathrm{all})}$, and $\sigma_p^{(\mathrm{all})}$ in Table VI. The differences between the results obtained with $V_p = 0.9V_n$ and $V_p = V_n$ are only 0.028 MeV for $\sigma_p^{(\mathrm{all})}$ and 0.009 MeV for $\sigma_n^{(\mathrm{all})}$. Here, the Skyrme SLy4 plus PDF-IV2 with $(\eta_0, \eta_2) = (0.75, 2.5)$ is used. The parameters η_1 and V_n are determined by the two-step procedure for both cases. The value of η_1 is 0.585 for $V_p = 0.9V_n$, and this is about two times larger than 0.270 for $V_p = V_n$.

In Fig. 10, the neutron pairing gaps in Ca, Ni, Sn, and Pb isotopes and the proton pairing gaps in $N = 20$, 28, 50, and 82 isotones are shown. We see that the two pair-DFs give almost the same results for both neutron and proton pairing gaps from the proton to neutron drip lines, if $N > Z$ is satisfied. This means that the weaker V_p can be compensated by the larger η_1 in the local pairing strength $V_p g_p[\rho, \rho_1] = V_p(1 + \eta_1\rho_1/\rho_0 + \cdots)$ in the case of $\rho_1 > 0$. This mechanism is absent in the pair-DF with only ρ dependence, and stronger V_p than V_n is needed.

In nuclei with $Z > N$, the calculation with $V_p = V_n$ gives larger proton pairing gaps compared to that with $V_p = 0.9V_n$. This is due to $\rho_1 < 0$. This means that the linear ρ_1 term in our pair-DF can mimic the Coulomb effect, but this approximation can be applied to nuclei with $N > Z$.

VI. CONCLUSION

We determined the pair-DF with ρ and ρ_1 dependences by analyzing all the experimental pairing gaps in even-even nuclei with $N, Z > 8$. For this purpose, we performed the extensive Hartree-Fock-Bogoliubov calculations with Skyrme force. Our pair-DF is promising for improving the global description of pairing correlations and pairing-sensitive observables due to the reproducibility of the mass number and neutron-excess dependence of the pairing gaps.

In this study, we advocate the use of the pair-DF determined by the two-step procedure. We found that the strong ρ dependence $\eta_0 \approx 0.75$ is commonly required for the Skyrme parametrizations: SLy4, SkM*, LNS, and SkP.

The empirical correlations among the V_0 and η_0 in the isoscalar part of our pair-DF and the isoscalar effective mass m_s/m of the particle-hole Skyrme force are extracted. Through these analyses, we found that the change of $\sigma_{\rm tot}^{\rm (all)}$ is less than 0.05 MeV when the parameter set (V_0, η_0) satisfies two conditions: $\eta_0 \geqslant 0.75$ and $|V_0| \leqslant |V_{\rm vac}|$.

Under these constraints, the isovector-density dependence η_1 is optimized for each (V_0, η_0) to minimize the uncertainties of the isovector terms η_1 and η_2. We pointed out that the available experimental information on pairing gaps in neutron-rich nuclei is not sufficient for accurate determination of the isovector part in the pair-DF. It is indispensable to continue to analyze upcoming experimental data for more neutron-rich nuclei and also the excited states for further extension of the pair-DF. This remains for future study.

We also discussed the Coulomb effect in the pairing channel. We showed that the linear ρ_1 term in the pair-DF can mimic the Coulomb reduction effect in neutron-rich nuclei. This means that the pair-DF with charge symmetry has the same global description power compared to the pairing force, including the explicit Coulomb effect. In this work, we showed the applicability of this prescription for the ground state only, but it is an interesting subject to clarify the Coulomb effect in excited states as well [63]. This will remain a future subject for quasiparticle RPA calculation with exact treatment of the Coulomb force [64].

We discussed finally the predictive power of the present pair-DF for pairing properties around drip-line regions in comparison with the pairing interaction $V_{\rm vac}$ determined by the neutron-neutron scattering length of $^1S_0$ channel.

ACKNOWLEDGMENTS

We are grateful to K. Matsuyanagi, M. Matsuo, T. Nakatsukasa, and K. Yabana for valuable discussions. This work was supported in part by the JSPS Core-to-Core Program, International Research Network for Exotic Femto Systems (EFES), a Grant-in-Aid for Scientific Research on Innovative Areas (No. 20105003), and the Japanese Ministry of Education, Culture, Sports, Science and Technology via a Grant-in-Aid for Scientific Research under the program numbers (C) 22540262 and 20540277. The numerical calculations were carried out on Altix3700 BX2 and SR16000 computers at the Yukawa Institute for Theoretical Physics in Kyoto University.

[1] M. Bender, P.-H. Heenen, and P.-G. Reinhard, Rev. Mod. Phys. **75**, 121 (2003).
[2] J. Terasaki, F. Barranco, R. A. Broglia, E. Vigezzi, and P. F. Bortignon, Nucl. Phys. A **697**, 127 (2002).
[3] D. J. Dean and M. Hjorth-Jensen, Rev. Mod. Phys. **75**, 607 (2003).
[4] F. Barranco, P. F. Bortignon, R. A. Broglia, G. Colo, P. Schuck, E. Vigezzi, and X. Vinas, Phys. Rev. C **72**, 054314 (2005).
[5] A. Pastore, F. Barranco, R. A. Broglia, and E. Vigezzi, Phys. Rev. C **78**, 024315 (2008).
[6] T. Duguet, Phys. Rev. C **69**, 054317 (2004).
[7] T. Duguet and T. Lesinski, Eur. Phys. J. Special Topics **156**, 207 (2008).
[8] A. Fabrocini, S. Fantoni, A. Yu. Illarionov, and K. E. Schmidt, Nucl. Phys. A **803**, 137 (2008).
[9] S. Gandolfi, A. Yu. Illarionov, S. Fantoni, F. Pederiva, and K. E. Schmidt, Phys. Rev. Lett. **101**, 132501 (2008).
[10] A. Gezerlis and J. Carlson, Phys. Rev. C **77**, 032801 (2008).
[11] L. G. Cao, U. Lombardo, and P. Schuck, Phys. Rev. C **74**, 064301 (2006).
[12] T. Duguet, T. Lesinski, K. Hebeler, K. Bennaceur, A. Schwenk, and J. Meyer, Int. J. Mod. Phys. E **18**, 2007 (2009).
[13] M. Kortelainen, T. Lesinski, J. More, W. Nazarewicz, J. Sarich, N. Schunck, M. V. Stoitsov, and S. Wild, Phys. Rev. C **82**, 024313 (2010).
[14] P. Klüpfel, P.-G. Reinhard, T. J. Burvenich, and J. A. Maruhn, Phys. Rev. C **79**, 034310 (2009).
[15] R. R. Chasman, Phys. Rev. C **14**, 1935 (1976).
[16] S. G. Kadmenskiĭ, Yu. L. Ratis, K. S. Rybak, and V. I. Furman, Sov. J. Nucl. Phys. **27**, 481 (1979).
[17] G. F. Bertsch and H. Esbensen, Ann. Phys. (NY) **209**, 327 (1991).
[18] J. Terasaki, P.-H. Heenen, P. Bonche, J. Dobaczewski, and H. Flocard, Nucl. Phys. A **593**, 1 (1995).
[19] Z. Bochnacki, I. M. Holban, and I. N. Mikhailov, Nucl. Phys. A **97**, 33 (1967).
[20] J. Dobaczewski, W. Nazarewicz, T. R. Werner, J. F. Berger, C. R. Chinn, and J. Dechargé, Phys. Rev. C **53**, 2809 (1996).
[21] J. Dobaczewski and W. Nazarewicz, Prog. Theor. Phys. Suppl. **146**, 70 (2002).
[22] J. Dobaczewski, W. Nazarewicz, and P.-G. Reinhard, Nucl. Phys. A **693**, 361 (2001).
[23] M. Yamagami, Y. R. Shimizu, and T. Nakatsukasa, Phys. Rev. C **80**, 064301 (2009).
[24] M. Yamagami and Y. R. Shimizu, Phys. Rev. C **77**, 064319 (2008).
[25] J. Margueron, H. Sagawa, and K. Hagino, Phys. Rev. C **76**, 064316 (2007).
[26] J. Margueron, H. Sagawa, and K. Hagino, Phys. Rev. C **77**, 054309 (2008).
[27] G. Audi, A. H. Wapstra, and C. Thibault, Nucl. Phys. A **729**, 337 (2003).
[28] P. Vogel, B. Jonson, and P. G. Hansen, Phys. Lett. B **139**, 227 (1984).
[29] X. Vinas, P. Schuck, and M. Farine, Int. J. Mod. Phys. E **20**, 399 (2011).
[30] J. Dobaczewski, H. Flocard, and J. Treiner, Nucl. Phys. A **422**, 103 (1984).
[31] E. Perlinska, S. G. Rohozinski, J. Dobaczewski, and W. Nazarewicz, Phys. Rev. C **69**, 014316 (2004).
[32] E. Chabanat, P. Bonche, P. Haensel, J. Meyer, and R. Schaeffer, Nucl. Phys. A **635**, 231 (1998); **643**, 441(E) (1998).
[33] J. Bartel, P. Quentin, M. Brack, C. Guet, and H.-B. Hakansson, Nucl. Phys. A **386**, 79 (1982).
[34] L. G. Cao, U. Lombardo, C. W. Shen, and N. V. Giai, Phys. Rev. C **73**, 014313 (2006).

[35] M. V. Stoitsov, J. Dobaczewski, W. Nazarewicz, and P. Ring, Comput. Phys. Commun. **167**, 43 (2005).
[36] M. Bender, K. Rutz, P.-G. Reinhard, and J. A. Maruhn, Eur. Phys. J. A **8**, 59 (2000).
[37] M. Yamagami, K. Matsuyanagi, and M. Matsuo, Nucl. Phys. A **693**, 579 (2001).
[38] M. Matsuo, Nucl. Phys. A **696**, 371 (2001).
[39] W. Satula, J. Dobaczewski, and W. Nazarewicz, Phys. Rev. Lett. **81**, 3599 (1998).
[40] G. F. Bertsch, C. A. Bertulani, W. Nazarewicz, N. Schunck, and M. V. Stoitsov, Phys. Rev. C **79**, 034306 (2009).
[41] C. A. Bertulani, H. F. Lu, and H. Sagawa, Phys. Rev. C **80**, 027303 (2009).
[42] T. Duguet, P. Bonche, P.-H. Heenen, and J. Meyer, Phys. Rev. C **65**, 014310 (2002); **65**, 014311 (2002).
[43] P. Ring and P. Schuck, *The Nuclear Many-Body Problem* (Springer-Verlag, Berlin, 1980).
[44] C. Baumer *et al*., Phys. Rev. C **71**, 044003 (2005).
[45] H. Esbensen, G. F. Bertsch, and K. Hencken, Phys. Rev. C **56**, 3054 (1997).
[46] K. Hagino and H. Sagawa, Phys. Rev. C **72**, 044321 (2005).
[47] N. Vinh Mau and J. C. Pacheco, Nucl. Phys. A **607**, 163 (1996).
[48] T. Oishi, K. Hagino, and H. Sagawa, Phys. Rev. C **82**, 024315 (2010); **82**, 069901(E) (2010).
[49] E. Garrido, P. Sarriguren, E. Moya de Guerra, and P. Schuck, Phys. Rev. C **60**, 064312 (1999).
[50] K. Bennaceur, J. Dobaczewski, and M. Ploszajczak, Phys. Lett. B **496**, 154 (2000).
[51] M. Matsuo, K. Mizuyama, and Y. Serizawa, Phys. Rev. C **71**, 064326 (2005).
[52] E. Khan, M. Grasso, and J. Margueron, Phys. Rev. C **80**, 044328 (2009).
[53] M. Matsuo and Y. Serizawa, Phys. Rev. C **82**, 024318 (2010).
[54] E. Pllumbi, M. Grasso, D. Beaumel, E. Khan, J. Margueron, and J. van de Wiele, Phys. Rev. C **83**, 034613 (2011).
[55] H. Shimoyama and M. Matsuo, Phys. Rev. C **84**, 044317 (2011).
[56] M. Grasso, D. Lacroix, and A. Vitturi, Phys. Rev. C **85**, 034317 (2012).
[57] E. Khan, J. Margueron, G. Colo, K. Hagino, and H. Sagawa, Phys. Rev. C **82**, 024322 (2010).
[58] M. Anguiano, J. L. Egido, and L. M. Robledo, Nucl. Phys. A **683**, 227 (2001).
[59] T. Lesinski, T. Duguet, K. Bennaceur, and J. Meyer, Eur. Phys. J. A **40**, 121 (2009).
[60] H. Nakada and M. Yamagami, Phys. Rev. C **83**, 031302(R) (2011).
[61] F. Tondeur, S. Goriely, J. M. Pearson, and M. Onsi, Phys. Rev. C **62**, 024308 (2000).
[62] M. Yamagami, Y. R. Shimizu, and T. Nakatsukasa, Mod. Phys. Lett. A **25**, 1923 (2010).
[63] T. Oishi, K. Hagino, and H. Sagawa, Phys. Rev. C **84**, 057301 (2011).
[64] H. Nakada, K. Mizuyama, M. Yamagami, and M. Matsuo, Nucl. Phys. A **828**, 283 (2009).